Theoretical investigation of magnons in Fe-Ga alloys

Gustav Johansson [*], Oleg I. Gorbatov, and Corina Etz
Applied Physics, Division of Material Science, Department of Engineering Sciences and Mathematics,
Luleå University of Technology, 97187 Luleå, Sweden

Fe–Ga alloys show an unusually large increase in magnetostriction compared to pure Fe and are one of the most interesting Fe-based alloys for this reason. However, the origin of the large magnetostriction and its relation to the chemical ordering on the underlying bcc phase is still under debate. To gain further understanding of the extraordinary magnetoelastic characteristics of this system, we investigate the effect of Ga-concentration and ordering on the spin-wave spectra and stiffness. The magnetic interactions in the Fe–Ga alloys are obtained by *ab initio* electronic structure calculations and the magnon spectra are modeled using atomistic spin dynamics modeling. Our results agree with available experimental data and show softening of the magnon modes with increasing Ga-concentration and a strong reduction of the spin-wave stiffness due to atomic ordering.

I. INTRODUCTION

The addition of nonmagnetic elements to body-centered cubic (bcc) Fe can strongly alter the anisotropy and enhance the magnetostriction [1–3]. Dilute alloys of Fe with Al, Ga, and Be all show enhancement of the tetragonal magnetostriction compared to bcc-Fe [1–6]. The largest enhancement is found for Ga, which is a factor of 15 over that of bcc-Fe [7], thus making these alloys very attractive to use in magnetostrictive actuators, sensors, and spintronic devices [8–10].

$Fe_{1-x}Ga_x$ has the inclination to retain local bcc-like symmetry both in the disordered A2 and in the ordered B2 and $D0_3$ phases [11] and has a phase diagram similar to other Fe-based binary alloys such as $Fe_{1-x}Si_x$ and $Fe_{1-x}Al_x$ [12]. It was shown that the Ga distribution, even in the disordered phase, is not completely random [13] and the short-range order increases with Ga content, leading to the ordered $D0_3$ phase occurring at $x \sim 0.25$ [13,14]. It has further been established that for both the ordered and disordered phases in these alloys, the magnetic properties on different Fe sites are strongly affected by the local atomic environment [15].

The maximum values of the tetragonal magnetostriction at room temperature occur at two peaks located at $x = 0.19$ and $x = 0.27$ [4,11,16]. Major efforts have been dedicated to investigating the mechanisms that lead to the large enhancement of magnetostriction. Both intrinsic mechanisms, meaning changes of the electronic structure induced by the nonmagnetic Ga atoms [17–19] and extrinsic mechanisms,

such as the formation of precipitation or nanoparticles [4,20–22], have been proposed. However, the origin of magnetostriction and its relation to chemical ordering on the underlying bcc lattice is still under debate.

Consequently, the majority of investigations have been focused on the ground-state properties [3,4,7,11–13,15–31] and only a few studies have considered the magnon and phonon spectra. These studies consist of early Mössbauer experiments, which estimated the exchange stiffness for different Ga-concentrations [14] and more recent neutron scattering experiments, which determined the phonon [32] and magnon spectra [33].

Magnon and phonon spectra are generally difficult to model for Fe-based alloys, and most theoretical efforts have only considered modeling ground-state properties using density functional theory (DFT) [18,19,22,25–30] and molecular dynamics [25,28]. Nevertheless, from a microscopic point of view, a complete characterization of atomic and magnetic interactions is highly desirable. There are a few theoretical investigations of spin dynamics for closely related Fe-based binary alloys [34–36]. The spin-wave spectra and the spin-wave stiffness were investigated in $Fe_{1-x}Al_x$ systems [34,35], while for the $Fe_{1-x}Si_x$ systems even the concentration dependence of the spin-wave stiffness was addressed [36]. However, to the best of our knowledge, no calculations of the magnon spectra in $Fe_{1-x}Ga_x$ have been carried out for the ferromagnetic disordered A2 and partially ordered $D0_3$ structures. This is important to describe and complement recent neutron scattering experiments [33].

The aim of our paper is to gain further knowledge of the interplay between the local atomic structure and magnetism in the dilute $Fe_{1-x}Ga_x$ alloys by examining ground-state properties and the low-energy excitation spectra via the Heisenberg exchange interactions. In particular, we investigate the concentration dependence of the spin-wave spectra and stiffness. An accurate description of the spin dynamics in this system would give insights into the magnetoelastic behavior in $Fe_{1-x}Ga_x$ alloys.
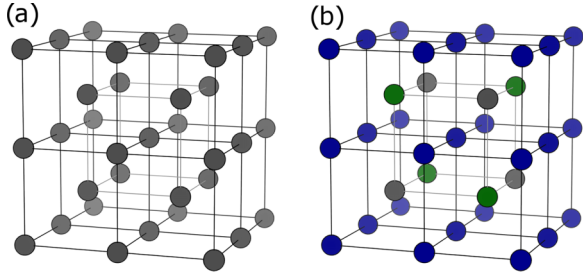
---

[*]gustav.johansson@ltu.se

FIG. 1. (a) The conventional cell of the disordered A2 structure where all positions are equivalent, partially occupied by both Fe and Ga (black). (b) The conventional cell of the (partially) ordered D0$_3$ structure where the 4a, 4b, and 8c positions are shown in black, green, and blue, respectively.

II. METHOD

The *ab initio* calculations were performed using the multiple-scattering approach of DFT as implemented in SPR-KKR [37]. The potential was treated in the atomic sphere approximation and the nonstoichiometric compositions were described within the coherent potential approximation (CPA). In the CPA approach, the alloy is replaced by an effective medium, and thus cannot take into account the effect of short-range order. However, modern implementations are not restricted to only one atom and allow for sub-stoichiometric systems [37–40]. Hence, by considering cells with more than one sublattice, it is possible to describe partially ordered structures having a fixed local environment around the partially occupied atom.

The structures are described in Fig. 1 and Table I, where the A2 structure (primitive bcc cell of one atom) has all sites equal and partially occupied by Fe and Ga. For the ordered and partially ordered D0$_3$ structure (primitive fcc cell of four atoms), we apply the following naming convention: Fe1 denotes the Fe atoms in the 4a position, which are partially occupied by Ga for $x < 0.25$, Fe2 denotes the Fe-atoms in the 4b position, and Fe3 denotes the Fe atoms at the 8c position.

It is well known that for 3d metals the exchange-correlation energy is better treated in the generalized gradient approximation (GGA) for structure optimization while magnetic properties are better treated in the local density approximation (LDA) [41]. Hence, the structure optimization was performed using GGA in the Perdew-Burke-Enzerhof parametrization [42], and all other calculations were performed using LDA in the parametrization of Vosko-Wilk-Nusair [43].

TABLE I. The atomic distribution for off-stoichiometric Fe$_{1-x}$Ga$_x$ in the A2 and D0$_3$ structures.

Space group	Wyckoff positions	Atoms
$Im\bar{3}m$ (No. 229)	4a: 0, 0, 0	Ga, Fe
	4a: 0, 0, 0	Ga, Fe1 ($x \leqslant 0.25$)
$Fm\bar{3}m$ (No. 225)	4b: 1/2, 1/2, 1/2	Fe2
	8c: 1/4, 1/4, 1/4	Fe3

Magnon spectra modeling are now routine calculations using, either time-dependent DFT (TDDFT) via the dynamical suceptibility [44–46] or by mapping the exchange energy to a Heisenberg Hamiltonian [47–56]. In particular, the Green's function formalism of TDDFT where the CPA method can be utilized [45,46] is very attractive for alloys. However, in this paper we are using the less computational demanding method of mapping the exchange coupling energy to a semiclassical Heisenberg Hamiltonian of individual pairs of localized moments $\mathbf{M}_{i\nu}$ and $\mathbf{M}_{j\mu}$ at sites i and j of type ν and μ, respectively,

$$\mathcal{H} = -\sum_{i\nu j\mu} J_{i\nu j\mu}\mathbf{M}_{i\nu} \cdot \mathbf{M}_{j\mu}. \tag{1}$$

The exchange coupling constants $J_{i\nu j\mu}$ were obtained by the magnetic force theorem using the relativistic extension [57] to the method of Liechtenstein *et al.* [53–55]. This formulation conveniently allows us to deal with disordered materials using CPA. Moreover, the method gives access to the full exchange tensor. However, only the symmetric part of the exchange tensor has been used in this paper.

With the calculated exchange parameters and the Heisenberg Hamiltonian defined in Eq. (1), the magnon spectra were determined using two different methods. At finite temperatures, we employ atomistic spin dynamics (ASD), where the dynamics of the magnetic moments are governed by Langevin dynamics through the coupled stochastic differential Landau-Lifschitz-Gilbert equations. By sampling the time and space correlation function

$$C^{\alpha\beta}(\mathbf{r}, t) = \frac{1}{N}\sum_{i,j}\left\langle M_i^\alpha(t)M_j^\beta(0)\right\rangle - \left\langle M_i^\alpha(t)\right\rangle\left\langle M_j^\beta(0)\right\rangle, \tag{2}$$

where α and β denote Cartesian coordinates. Taking the double Fourier transform, we get an estimate of the dynamical structure factor $S^{\alpha\beta}(\mathbf{q}, \omega)$. The magnon energies are then given by the peak values of $S^{\alpha\beta}(\mathbf{q}, \omega)$ at each wave vector $\mathbf{q}$.

We also calculate the adiabatic magnon spectra valid for close to zero temperature. We follow the approach of Kübler [56] and consider the expression for a spin-spiral configuration

$$\mathbf{M}_{i\nu} = M_\nu[\sin\theta_\nu \cos(\mathbf{q} \cdot (\mathbf{R}_i + \boldsymbol{\tau}_\nu) + \varphi_\nu)\mathbf{e}_x$$
$$+ \sin\theta_\nu \sin(\mathbf{q} \cdot (\mathbf{R}_i + \boldsymbol{\tau}_\nu) + \varphi_\nu)\mathbf{e}_y + \cos\theta\mathbf{e}_z], \tag{3}$$

where M_ν is the magnitude of the magnetic moment at site $\boldsymbol{\tau}_\nu$, $\mathbf{R}_i$ is a translation vector, $\mathbf{q}$ is the wave vector characterizing the spin-spiral, θ_ν is the cone angle, and φ_ν is a phase difference. With the time evolution of the localized magnetic moments given by the Landau-Lifshitz equations and assuming small cone angles θ_ν, we get a linear system of equations given by

$$\omega\theta_\nu = 4\sum_\mu[J_{\nu\mu}(\mathbf{q})\theta_\mu M_\mu x_\mu - J_{\nu\mu}(\mathbf{0})\theta_\nu M_\nu x_\nu], \tag{4}$$

where we have introduced the Fourier transform of the exchange parameters $J_{\nu\mu}(\mathbf{q})$. The parameters x_ν and x_μ correspond to the chemical concentration for atom type ν and μ, respectively.

An alternative method was presented by Buczek *et al.* [50] in which the transverse susceptibility is parameterized by exchange parameters from CPA calculations. This is indeed a very interesting method. However, it seems unlikely that it can properly account for correlated disorder, in the way it is presented, with exchange parameters from single-site CPA calculations. The exchange parameters are strongly affected by the local environment, as shown below, and this should be included in the modeling. Nonetheless, for completely disordered phases we expect similar results to our method.

There exist several techniques to extract the spin stiffness [34,53–55,58,59]. However, in this paper the stiffness D was estimated using least-squares fitting of the quadratic energy dispersion relation, $\hbar\omega = Dq^2$. This method is expected to give similar results to the methods used for the Fe–Si and Fe–Al systems [34,36].

Computational details

The KKR calculations were performed using a basis set consisting of *spdf* orbitals for the expansion of the Green's function. The energy integration of the Green's function was done with 32 energy points along a semicircle contour, and the Brillouin zone (BZ) was sampled with a $31 \times 31 \times 31$ and $25 \times 25 \times 25$ k-point mesh for the A2 and D0$_3$ calculations respectively. For the calculations of the exchange constants, a very dense set of k points was used, $81 \times 81 \times 81$ and $69 \times 69 \times 69$, for the A2 and D0$_3$ structure respectively. It should be noted here that all results were checked carefully by increasing the k-point grid and the energy points.

In the ASD simulations, the alloys were treated using large supercells in which each site was chemically randomly occupied according to the concentration (see Table I). It should be noted that we obtain a small induced moment on the Ga atoms from the *ab initio* calculations. Induced moments are not well described within the Heisenberg model. Hence, in the ASD simulations, we replace the Ga atoms with vacancies. The ASD simulations were performed using UPPASD software [60]. To represent most of the local environments, we use large supercells $60 \times 60 \times 60$ for the A2 structures and $40 \times 40 \times 40$ for the D0$_3$ structures.

III. RESULTS AND DISCUSSION

The exchange coupling parameters and magnetic moments are generally dependent on the distance between the atoms. As is well-known for bcc-Fe, the magnetic moment increases linearly with the lattice parameter around equilibrium as the magnetic moment becomes more localized [61,62]. The trend is the opposite for the exchange interaction, with the exchange energy decreasing for more separated atoms. Thus, it will affect the calculations of the magnon spectra. To this end, we begin this section by presenting results for lattice parameter optimization.

A. Structure and ground state properties

In Fig. 2, the optimized lattice parameters a, as a function of Ga concentration together with experimental values [13,14,63,64] are shown. The optimized lattice parameters were found by fitting total energies to a Murnaghan
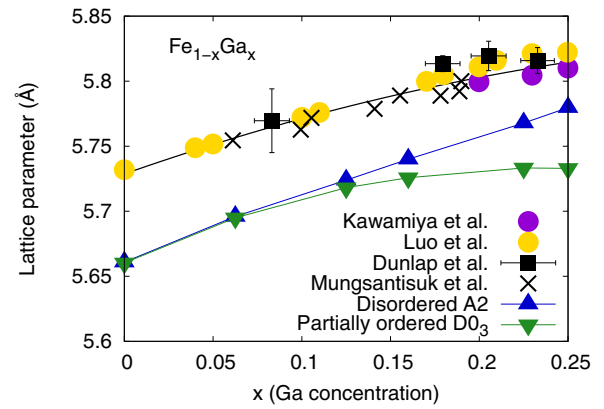

FIG. 2. Calculated lattice parameters as a function of Ga concentration together with experimental values from Kawamiya *et al.* [14], Luo [63], Dunlap *et al.* [13], Mungsantisuk *et al.* [64], and the references therein. The lattice parameters for the A2 structures are multiplied by two to compare with the lattice parameters of the D0$_3$ structures. The black line represents interpolated values of the experimental data and the blue and green lines are mere guidelines.

equation of states [65]. The calculated lattice parameters are generally shifted to lower values compared to experimental data (~ 0.07 Å). This corresponds to an error of approximately 1% and is similar for both structures. More importantly are the trends seen in the A2 and D0$_3$ structures. The simulated values for the A2 structure show a linear trend with increasing Ga content and thus follow Vegard's law. The same is seen for the D0$_3$ simulations up to $x \sim 0.15$, after which it deviates slightly. It is more difficult to distinguish a general trend from the collective experimental data, from different sources measured in slightly different conditions. However, the best fitting polynomial was a second-order polynomial. All other calculations in this paper are based on the experimental lattice parameters and the polynomial is used to interpolate between intermediate concentrations.

Using the experimental lattice parameters, we calculate the magnetic moments. The results are shown in Fig. 3. The
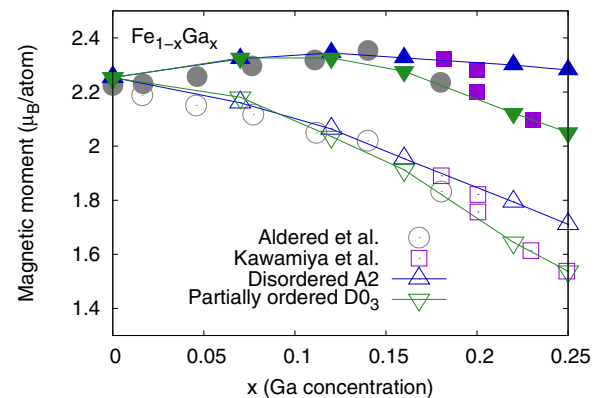

FIG. 3. Calculated magnetic moment as a function of Ga concentration together with experimental values from Aldred [66] and Kawamiya *et al.* [14]. Filled symbols represent the average magnetic moment per Fe atom, and open symbols represent the total average magnetic moment per atom.
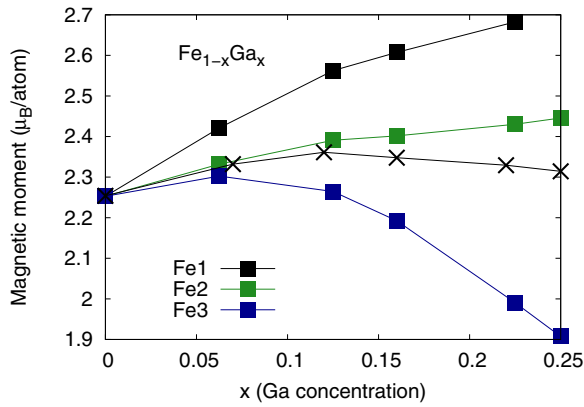
FIG. 4. Calculated magnetic moment as a function of Ga concentration for Fe atoms on different sublattices. Filled symbols represent the magnetic moment for the $D0_3$ structure and crosses represent the A2 structure (see Fig. 1 and Table I).
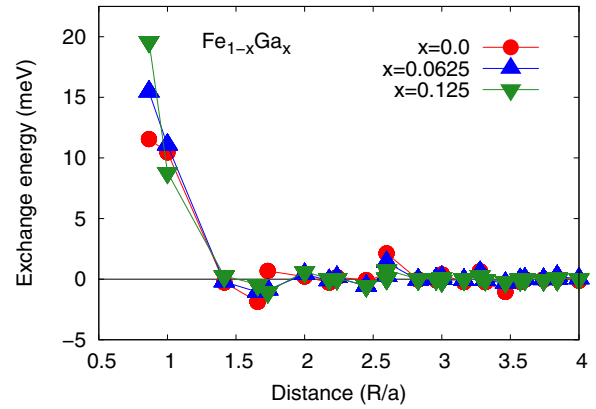

FIG. 5. Exchange coupling parameters within four lattice parameters for three different concentrations of the A2 structure. The lines are added for guiding purposes.

figure shows the total average magnetic moment per atom (open symbols) as well as the total average magnetic moment per Fe atom (filled symbols) for both structures. The figure also shows experimental results from Aldred [66] and Kawamiya *et al.* [14]. It should be mentioned here that the calculations show a small induced antiparallel magnetic moment on the Ga atoms of around -0.1 μ_B. This induced moment, however, changes very little with concentration.

In Fig. 3, it is seen that the average moment per atom is reduced with increasing Ga content; however, not as linearly as expected when diluting the magnetic Fe atoms with nonmagnetic Ga atoms. The average moment per iron atom increases with the addition of Ga atoms with a maximum of nearly 2.4 μ_B for $x = 0.16$. The A2 results fit experimental data very well for lower concentrations ($x < 0.15$). For larger concentrations ($x > 0.15$), the A2 moments start to deviate while the $D0_3$ moments follow the experimental ones closely. The concentration dependence can be traced back to changes induced by solute atoms in the local electronic and magnetic structure, as has been previously discussed for the Fe-based systems [15,67–69]. The magnetic moments strongly depend on the local environment of the interacting atoms in the matrix and depends on the number of solute nearest neighbors [67,68].

The local magnetic moments on the different sublattices are presented in Fig. 4. While the induced antiparallel moment on the Ga atoms remains relatively small, the effect on the Fe atoms is substantial. The Fe2 atoms (Wyckoff position 4*b*), which have Ga atoms in the second coordination sphere, are seen to be less affected by the presence of the Ga atom and almost constant with increasing Ga concentrations. However, the magnetic moments on the Fe3 atoms (Wyckoff position 8*c*), which have Ga atoms in the first coordination sphere, are affected to a large degree and reduced by around 20% at $x = 0.25$. The magnetic moment of the Fe1 atoms (Wyckoff position 4*a*) shows the opposite trend with increasing magnetic moment for increasing Ga concentration (12% increase for $x = 0.225$). The Fe1 atoms for $x < 0.25$ have Ga atoms only in the third coordination sphere. The magnetic moment is thus very dependent on the local environment despite the

delocalized nature of the *d* electrons. This has also been noted in the case of $Fe_{1-x}Si_x$ [70]. Similar to $Fe_{1-x}Ga_x$, the $Fe_{1-x}Si_x$ alloys show a strong dependence of magnetic properties with Si concentration with local magnetic moments at Fe sites that may become higher than in pure iron depending on the distribution of Fe and Si neighbors. In particular, they show that also the influence of the second and third coordination sphere plays a big part in the local magnetic moment. It should be noted that the nonmonotonic behavior of the concentration dependence for the average magnetic moment in alloys can also be explained in the classical consideration by exchange interactions with different signs between alloy components [71]. Considering the spins of atoms as classical vectors, the magnetic moment of the alloy is determined by the average values of the projections of atomic moments. An increase in the concentration of a dissolved element leads to an increase in pairs of atoms with negative interactions, which leads to a decrease in the projection of magnetic moments [71].

B. Magnetic exchange interaction

The magnetic exchange coupling parameters for different Ga concentrations were also calculated. The exchange parameters within a range of four lattice constants for the A2 structure are presented in Fig. 5. The largest interactions are the ones within the first and second coordination spheres. The interactions in the first coordination sphere are increasing with increasing Ga concentration, while the interactions in the second coordination sphere are decreasing. The other interactions are considerably smaller but nonzero for quite large distances. Nonetheless, this implies that the exchange interaction gets more short-ranged with increasing Ga content.

The behavior of the long-range interactions is well-known for bcc-Fe [72] and is seen to be less distinct with increasing Ga concentration. Only Fe-Fe interactions are shown, but as mentioned above, we get an induced moment on the nonmagnetic Ga atoms. Consequently, there are nonzero Ga-Ga and Fe-Ga exchange interactions. However, they are small and do not change much with Ga-content. The strongest interaction ($\sim$0.3 eV) is for Fe-Ga and is comparable to Fe-Fe interactions in the sixth coordination sphere. It should be noted that there have been attempts to include interactions
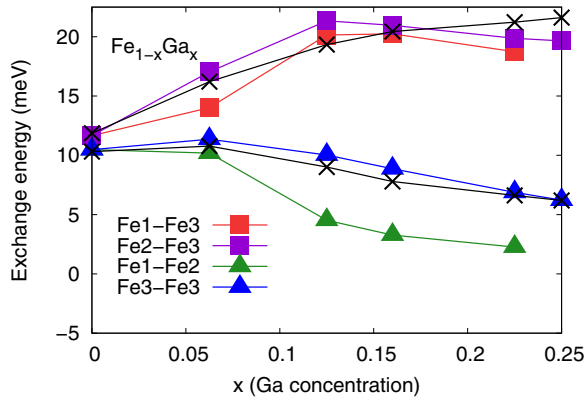
FIG. 6. Exchange coupling parameters for the two nearest-neighbor interactions with respect to Ga concentration. Crosses correspond to interactions in the A2 structure. The filled symbols correspond to interactions for the $D0_3$ structure, with the colors representing interactions between Fe-atoms on different sub-lattices. Squares and triangles represent interactions in the first and second shells, respectively (see Fig. 1 and Table I).

involving induced moments by introducing effective exchange interactions [73]. This, however, has not been considered in this paper.

For the A2 structure, the interaction is only between equivalent atoms. However, for the $D0_3$ structure, it is more complex. This is shown in Fig. 6 for interactions in the first and second coordination spheres. The colored symbols correspond to the exchange interaction between different sub-lattices for the $D0_3$ structure, and the crosses correspond to the A2 structure. The trend of the nearest-neighbor interactions is also seen for the partially ordered $D0_3$ structures.

The largest difference compared to the A2 structure is found in the second coordination sphere. It is seen that the Fe3-Fe3 interaction, more or less, follows the A2 interactions in size. The Fe1-Fe2 interaction, on the other hand, is much lower. However, the probability of this interaction appearing decreases with increasing Ga concentration and becomes zero for $x = 0.25$ when Ga atoms fully occupy the $4a$ lattice i.e., in an ordered phase.

C. Spin-wave spectra and stiffness

Complete measurements of the magnon dispersion relation of iron and iron-based systems by neutron scattering are difficult because the excitation spectrum extends to very high energies. The spin-wave spectra is known to be strongly affected by interactions with the Stoner continuum, which give rise to the so-called Landau damping of the collective magnon modes. This is well described by TDDFT calculations of the dynamical transverse susceptibility [44–46]. Obviously this is missing in the adiabatic approach employed here, which is only expected to be accurate in the long-wavelength limit. However, it is less computationally demanding and very useful in combination with other methods.

The adiabatic spin-wave spectra was calculated by finding the eigenvalues of the dynamical matrix in Eq. (4). The spin-wave stiffness was also based on the adiabatic spectra (see the end of this section), and the number of exchange parameters
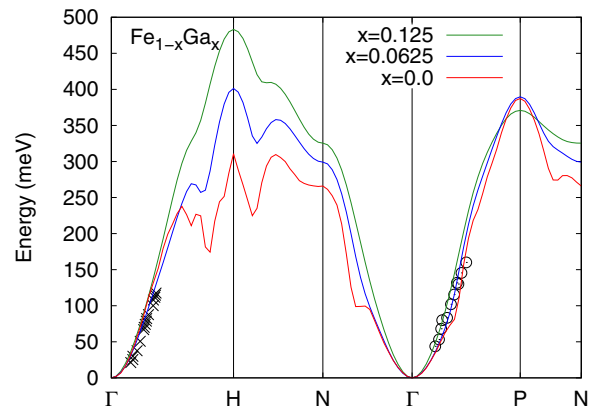

FIG. 7. Magnon spectra for three different concentrations in the A2 phase together with experimental results measured at 10 K for bcc-Fe [75] (circles) and at room temperature for $Fe_{0.88}Si_{0.12}$ [76] (crosses). The color scheme is the same as in Fig. 5

used in these calculations is based on the convergence of the spin-wave stiffness. The spin-wave spectra and, thus, the spin-wave stiffness are very sensitive to the number of exchange parameters included [74]. This is due to the slowly decaying, oscillating behavior found for the exchange parameters in bcc-Fe (Fig. 5). Convergent results for the stiffness were achieved by including all exchange interactions up to $10 \times a$ for A2 and $5 \times a$ for $D0_3$.

The adiabatic spectra for low concentrations in the A2 phase are presented in Fig. 7. Although the shape of the magnon dispersions for bcc-Fe are similar to other theoretical results using the adiabatic approach [47–49,52], the bandwidth at H is considerably lower than expected (≈ 100 meV). However, due to the limitations of the adiabatic approach, the results further from the Γ point are questionable and no experimental data exists for validation of calculated results. Moreover, the spectra closer to the BZ edges were found to be extremely sensitive to the number of exchange parameters included in Eq. (1). Hence, since the presented results are converged with respect to the spin-wave stiffness in the long wavelength limit for which the theory should be correct, this deviation is not very surprising.

Regarding the effect of Ga concentrations, the Kohn anomalies that are very distinct for bcc-Fe are seen to be smeared out with higher Ga content. In addition, the dispersion curves at the H and N high-symmetry points are seen to increase with increasing Ga content and decrease at P, which is related to the large increase of the nearest-neighbor interaction (see Figs. 5 and 6).

Figure 7 also shows experimental results measured at 10 K for bcc-Fe [75] along the Γ-P direction and at room temperature for $Fe_{0.88}Si_{0.12}$ [76] along the Γ-H direction. For such low concentrations, there are only small changes in the spectra at low energies, and the experimental values are seen to fit reasonably well to the calculated ones.

In addition to smearing of the magnon modes due to Landau damping, increasing dilution of nonmagnetic atoms, or rather increasing disorder will also lead to broadening of the magnon dispersions. While this is not seen in the case of the adiabatic spectra, it is very obvious when calculating
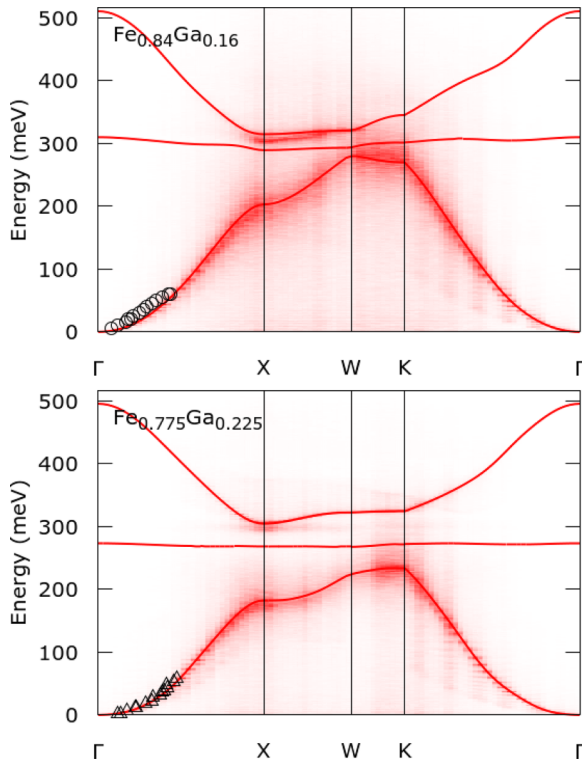
FIG. 8. Calculated spin-wave dispersion for a temperature of 4.2 K in the $D0_3$ phase. Red lines show adiabatic dispersion. Experimental values (black circles and triangles) from Zarestky *et al.* [33].
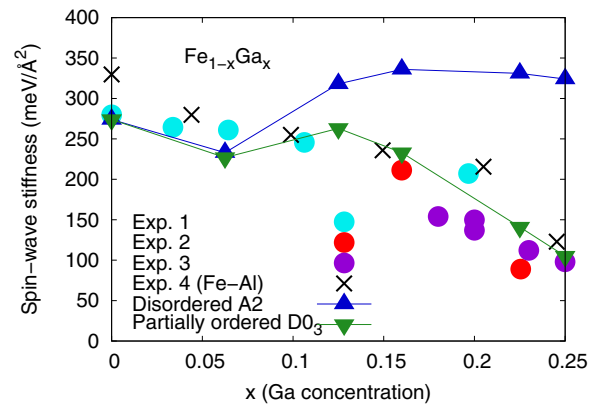

FIG. 9. Calculated spin-wave stiffness as a function of Ga concentration for disordered A2 and partially ordered $D0_3$. Experimental values from Antonini *et al.* [77] (Exp. 1), Zarestky *et al.* [33] (Exp. 2), Kawamiya *et al.* [14] (Exp. 3), and references in Ref. [34] (Exp. 4).

the spectra from the correlation function in ASD. This can be seen for two different $D0_3$ compositions in Fig. 8 where the dispersion curve is more spread out for the more disordered case ($x = 0.16$).

Another reason for the broadening originates from finite-temperature effects, which are included in terms of the stochastic fields and the Gilbert damping parameter. However, in this case, these effects should be relatively small since they are calculated for low temperatures ($T = 4.2$ K) to replicate the experimental values (black symbols) by Zarestky *et al.* [33].

Figure 8 also shows the magnon dispersions calculated in the adiabatic approximation (solid lines). These are seen to match the dispersions from ASD very well at this low temperature. Moreover, the experimental values are seen to fit very well to the calculated spectra, in particular, for the more ordered case of $Fe_{0.775}Ga_{0.225}$. A flattening of the bands can be seen for increasing Ga concentration, leading to an increase of the band gap. In particular, this is seen for the acoustic branch around the Γ point, which should be well described by our approach. The flattening of the acoustic branch is also found experimentally and indicates a reduction of the spin-wave stiffness.

The spin-wave stiffness was evaluated for the [110] direction to be consistent with recent experimental results [33]. Since the energy dispersion is only quadratic for small q around the Γ point, the interval used in the fitting was decreased until convergence was obtained.

The calculated spin-wave stiffness as a function of Ga concentration is shown in Fig. 9 together with experimental results from Antonini and Stringfellow [77], Zarestky *et al.* [33], and Kawamiya *et al.* [14]. For low concentrations, the disordered A2 structure follows the experimental values quite well. However, for higher concentrations, it deviates considerably and increases in size in contrast to experiments. The same trend has also been found for $Fe_{1-x}Al_x$ [34,35], where after an initial decrease in stiffness with a minimum at $x = 0.05$, the stiffness increases and saturates around $x = 0.2$. Similar behavior was also found for $Fe_{1-x}Si_x$ [36], but deviating even more from experimental values.

The deviation from experiments has been assigned to long-range chemical order found in the B2 and $D0_3$ structures for larger concentrations [34]. In Fig. 9, it is also seen that the fit is much better for the partially ordered $D0_3$ calculations, in particular for larger concentrations, thus strengthening the claims regarding the importance of structural order in the magnetic properties of diluted Fe-based alloys. It should also be noted here that our method of calculating the adiabatic magnon spectra and extracting the stiffness constant also seems to work well compared to other arguably more involved methods.

The spin-wave stiffness results that stand out most compared to experiments are the ones for $x = 0.0625$. Even though similar trends were found in previous related studies [34,35], spin-wave stiffness calculations for the arguably simpler case of bcc-Fe are very sensitive [59]. It is also known that short-range order is found even in the disordered A2 phase and increases with Ga content, leading to the ordered $D0_3$ phase [13]. However, in the present calculations, short-range order is only included for the partially ordered $D0_3$ structure in the sense that the length scale of the pair correlations goes to infinity and thus forms long-range chemical order.

For the low temperatures investigated here, the effects on the magnon spectra would be rather small compared to spin-flip excitations. It should nonetheless be commented on. It is known that Fe–Ga alloys demonstrate the interplay between magnetic and chemical ordering [15] where the chemical

ordering can be qualitatively different above and below the Curie temperature [78]. The electronic contribution to the free energy can be added as a thermal electron excitation [79] by including the Fermi–Dirac distribution to the *ab initio* calculations. This is, however, not considered here. Temperature effects are only considered in the form of spin temperature, included in terms of the Boltzmann distribution in Monte Carlo simulations and the stochastic fields in the Landau-Lifschitz equations. Hence, lattice excitations, e.g., phonons, are not included, which, in some cases, can be important [15]. However, magnon-phonon coupling is known to be relatively small in bcc-Fe [80]. This is likely also the case when diluting bcc-Fe with Ga since the magnon and phonon branches are well separated [32,33]. Nonetheless, such theoretical investigation would be very interesting and is left for future work.

IV. CONCLUSIONS

In this paper, the spin-wave spectra of dilute $Fe_{1-x}Ga_x$ alloys were considered for compositions up to $x = 0.25$. Two different phases were investigated, including the disordered A2 phase, which is known to be found in the dilute limit ($x \sim 0$) as well as the partially ordered $D0_3$ phase, found around $x = 0.25$. The ground-state magnetic properties were calculated using the fully relativistic Korringa-Kohn-Rostocker method in the atomic sphere approximation, where disorder was included by means of the CPA.

Mapping the exchange energy to a semiclassical Heisenberg Hamiltonian, the spin-wave spectra were calculated using ASD, where the nonstoichiometric compositions were represented using large supercells. In addition, the adiabatic spin-wave spectra were calculated, where disorder was included by configurational averages of the exchange parameters. This approach was seen to work very well for the Fe–Ga system, with a good fit to experimental results. The same could be seen in the spin-wave stiffness, which was estimated by a quadratic fit around the Γ point.

The results strongly suggest the importance of atomic ordering since the partially ordered calculations generally better fit experimental results. This is in spite of not including short-range order in the calculations, which could be important, especially in the A2 phase. Nonetheless, the calculations overall give a correct picture of the concentration dependence of the spin-wave spectra and stiffness.

The present paper neglects the presence of Landau damping and leaves unanswered the question about the vibrational free-energy contribution to the magnon spectrum. The questions of whether the effect of lattice vibrations on the magnon spectrum is large or not and how to accurately model the short-range order and correctly take it into account in the magnon spectra modeling call for further investigations.

[1] R. C. Hall, J. Appl. Phys. **30**, 816 (1959).

[2] R. C. Hall, J. Appl. Phys. **31**, 1037 (1960).

[3] A. E. Clark, J. B. Restorff, M. Wun-Fogle, T. A. Lograsso, and D. L. Schlagel, IEEE Trans. Magn. **36**, 3238 (2000).

[4] A. E. Clark, M. Wun-Fogle, J. B. Restorff, T. A. Lograsso, and J. R. Cullen, IEEE Trans. Magn. **37**, 2678 (2001).

[5] A. E. Clark, M. Wun-Fogle, J. B. Restorff, T. Lograsso, and G. Petculescu, J. Appl. Phys. **95**, 6942-6944 (2004).

[6] A. E. Clark, J. B. Restorff, M. Wun-Fogle, D. Wu, and T. Lograsso, J. Appl. Phys. **103**, 07B310 (2008).

[7] E. M. Summers, T. Lograsso, and M. Wun-Fogle, J. Mater. Sci. **42**, 9582 (2007).

[8] G. Petculescu, R. Wu, and R. McQueeney, Handb. Magn. Mater. **20**, 123 (2012).

[9] J. Atulasimha and A. B. Flatau, Smart Mater. Struct. **20**, 043001 (2011).

[10] S. Dutta, D. E. Nikonov, S. Manipatruni, I. A. Young, and A. Naeemi, Sci. Rep. **7**, 1 (2017).

[11] A. E. Clark, K. B. Hathaway, M. Wun-Fogle, J. B. Restorff, T. Lograsso, V. M. Keppens, G. Petculescu, and R. A. Taylor, J. Appl. Phys. **93**, 8621 (2003).

[12] O. Ikeda, R. Kainuma, I. Ohnuma, K. Fukamichi, and K. Ishida, J. Alloys Compd. **347**, 198 (2002).

[13] R. A. Dunlap, J. D. McGraw, and S. P. Farrell, J. Magn. Magn. Mater. **305**, 315 (2006).

[14] N. Kawamiya, K. Adachi, and Y. Nakamura, J. Phys. Soc. Jpn. **33**, 1318 (1972).

[15] O. I. Gorbatov, Y. N. Gornostyrev, P. A. Korzhavyi, and A. V. Ruban, Phys. Met. Metallogr. **117**, 1293 (2016).

[16] T. A. Lograsso, A. R. Ross, D. L. Schlagel, A. E. Clark, and M. Wun-Fogle, J. Alloys Compd. **350**, 95 (2003).

[17] T. Khmelevska, S. Khmelevskyi, and P. Mohn, J. Appl. Phys. **103**, 073911 (2008).

[18] C. Paduani and C. Bormio-Nunes, J. Appl. Phys. **109**, 033705 (2011).

[19] H. Wang, Y. N. Zhang, T. Yang, Z. D. Zhang, L. Z. Sun, and R. Q. Wu, Appl. Phys. Lett. **97**, 262505 (2010).

[20] A. G. Khachaturyan and D. Viehland, Metall. Mater. Trans. A **38**, 2308 (2007).

[21] J. X. Cao, Y. N. Zhang, W. J. Ouyang, and R. Q. Wu, Phys. Rev. B **80**, 104414 (2009).

[22] Y. N. Zhang, J. X. Cao, and R. Q. Wu, Appl. Phys. Lett. **96**, 062508 (2010).

[23] M. Wuttig, L. Dai, and J. Cullen, Appl. Phys. Lett. **80**, 1135 (2002).

[24] G. Petculescu, J. B. LeBlanc, M. Wun-Fogle, J. B. Restorff, W. C. Burton, J. X. Cao, R. Q. Wu, W. M. Yuhasz, T. A. Lograsso, and A. E. Clark, IEEE Trans. Magn. **45**, 4149 (2009).

[25] H. Wang, Z. D. Zhang, R. Q. Wu, and L. Z. Sun, Acta Mater. **61**, 2919 (2013).

[26] Y. N. Zhang, J. X. Cao, and R. Q. Wu, IEEE Trans. Magn. **47**, 4044 (2011).

[27] Y. Zhang, H. Wang, and R. Wu, Phys. Rev. B **86**, 224410 (2012).

[28] H. Wang, Y. N. Zhang, R. Q. Wu, L. Z. Sun, D. S. Xu, and Z. D. Zhang, Sci. Rep. **3**, 3521 (2013).

[29] R. Wu, J. Appl. Phys. **91**, 7358 (2002).

[30] X. Wang, R. Wu, D.-S. Wang, and A. J. Freeman, Phys. Rev. B **54**, 61 (1996).

[31] M. Matyunina, M. Zagrebin, V. Sokolovskiy, and V. Buchelnikov, EPJ Web Conf. **185**, 04013 (2018).

[32] J. L. Zarestky, V. O. Garlea, T. A. Lograsso, D. L. Schlagel, and C. Stassis, Phys. Rev. B **72**, 180408(R) (2005).

[33] J. L. Zarestky, O. Moze, J. W. Lynn, Y. Chen, T. A. Lograsso, and D. L. Schlagel, Phys. Rev. B **75**, 052406 (2007).

[34] I. Turek, J. Kudrnovský, and V. Drchal, Phys. Rev. B **101**, 134410 (2020).

[35] P. Buczek, L. M. Sandratskii, N. Buczek, S. Thomas, G. Vignale, and A. Ernst, Phys. Rev. B **94**, 054407 (2016).

[36] M. Rinaldi, M. Mrovec, M. Fähnle, and R. Drautz, Phys. Rev. B **104**, 064413 (2021).

[37] H. Ebert, SPRKKR package, https://www.ebert.cup.uni-muenchen.de/index.php/en/software-en/13-sprkkr.

[38] A. J. Pindor, W. M. Temmerman, and B. L. Gyorffy, J. Phys. F: Met. Phys. **13**, 1627 (1983).

[39] N. H. Long, M. Ogura, and H. Akai, J. Phys.: Condens. Matter **21**, 064241 (2009).

[40] A. Bansil and S. Kaprzyk, Phys. Rev. B **43**, 10335 (1991).

[41] A. V. Ruban and I. A. Abrikosov, Rep. Prog. Phys. **71**, 046501 (2008).

[42] J. P. Perdew, K. Burke, and M. Ernzerhof, Phys. Rev. Lett. **77**, 3865 (1996).

[43] S. H. Vosko, L. Wilk, and M. Nusair, Can. J. Phys. **58**, 1200 (1980).

[44] T. Skovhus and T. Olsen, Phys. Rev. B **103**, 245110 (2021).

[45] J. B. Staunton, J. Poulter, B. Ginatempo, E. Bruno, and D. D. Johnson, Phys. Rev. B **62**, 1075 (2000).

[46] P. Buczek, A. Ernst, P. Bruno, and L. M. Sandratskii, Phys. Rev. Lett. **102**, 247206 (2009).

[47] S. V. Halilov, A. Y. Perlov, P. M. Oppeneer, and H. Eschrig, Europhys. Lett. **39**, 91 (1997).

[48] S. V. Halilov, H. Eschrig, A. Y. Perlov, and P. M. Oppeneer, Phys. Rev. B **58**, 293 (1998).

[49] M. van Schilfgaarde and V. P. Antropov, J. Appl. Phys. **85**, 4827 (1999).

[50] P. Buczek, S. Thomas, A. Marmodoro, N. Buczek, X. Zubizarreta, M. Hoffmann, T. Balashov, W. Wulfhekel, K. Zakeri, and A. Ernst, J. Phys.: Condens. Matter **30**, 423001 (2018).

[51] A. Jacobsson, G. Johansson, O. I. Gorbatov, M. Ležaić, B. Sanyal, S. Blügel, and C. Etz, Sci. Rep. **12**, 18987 (2022).

[52] F. L. Durhuus, T. Skovhus, and T. Olsen, J. Phys.: Condens. Matter **35**, 105802 (2023).

[53] A. I. Liechtenstein, M. I. Katsnelson, V. P. Antropov, and V. A. Gubanov, J. Phys. F: Met. Phys. **14**, L125 (1984).

[54] A. I. Liechtenstein, M. I. Katsnelson, V. P. Antropov, and V. A. Gubanov, J. Magn. Magn. Mater. **54-57**, 965 (1986).

[55] A. I. Liechtenstein, M. I. Katsnelson, V. P. Antropov, and V. A. Gubanov, J. Magn. Magn. Mater. **67**, 65 (1987).

[56] J. Kübler, *Theory of Itinerant Magnetism*, 2nd ed. (Oxford University Press, New York, 2009).

[57] H. Ebert and S. Mankovsky, Phys. Rev. B **79**, 045209 (2009).

[58] M. Pajda, J. Kudrnovský, I. Turek, V. Drchal, and P. Bruno, Phys. Rev. B **64**, 174402 (2001).

[59] O. Šipr, S. Mankovsky, and H. Ebert, Phys. Rev. B **101**, 174401 (2020).

[60] O. Eriksson, L. Bergman, L. Bergqvist, and J. Hellsvik, Uppsala Atomistic Spin Dynamics software, https://physics.uu.se/uppasd.

[61] D. Bagayoko and J. Callaway, Phys. Rev. B **28**, 5419 (1983).

[62] V. L. Moruzzi, Phys. Rev. Lett. **57**, 2211 (1986).

[63] H. L. Luo, AIME Met. Soc. Trans. **239**, 119 (1967).

[64] P. Mungsantisuk, R. P. Corson, and S. Guruswamy, J. Appl. Phys. **98**, 123907 (2005).

[65] C-L. Fu and K.-M. Ho, Phys. Rev. B **28**, 5480 (1983).

[66] A. T. Aldred, J. Appl. Phys. **37**, 1344 (1966).

[67] O. I. Gorbatov, I. K. Razumov, Y. N. Gornostyrev, V. I. Razumovskiy, P. A. Korzhavyi, and A. V. Ruban, Phys. Rev. B **88**, 174113 (2013).

[68] P. A. Korzhavyi, A. V. Ruban, J. Odqvist, J.-O. Nilsson, and B. Johansson, Phys. Rev. B **79**, 054202 (2009).

[69] N. Hamada, J. Phys. Soc. Jpn. **46**, 1759 (1979).

[70] N. G. Zamkova, V. S. Zhandun, S. G. Ovchinnikov, and I. S. Sandalov, J. Alloys Compd. **695**, 1213 (2017).

[71] S. K. Sidorov and A. V. Doroshenko, Phys. Status Solidi (b) **16**, 737 (1966).

[72] I. Turek, J. Kudrnovský, V. Drchal, and P. Bruno, Philos. Mag. **86**, 1713 (2006).

[73] S. Polesya, S. Mankovsky, O. Sipr, W. Meindl, C. Strunk, and H. Ebert, Phys. Rev. B **82**, 214409 (2010).

[74] C. Etz, L. Bergqvist, A. Bergman, A. Taroni, and O. Eriksson, J. Phys.: Condens. Matter **27**, 243202 (2015).

[75] C-K. Loong, J. M. Carpenter, J. W. Lynn, R. A. Robinson, and H. A. Mook, J. Appl. Phys. **55**, 1895 (1984).

[76] J. W. Lynn, Phys. Rev. B **11**, 2624 (1975).

[77] B. Antonini and M. W. Stringfellow, Proc. Phys. Soc. **89**, 419 (1966).

[78] M. W. Petrik, O. I. Gorbatov, and Y. N. Gornostyrev, JETP Lett. **98**, 809 (2014).

[79] K. Wildberger, P. Lang, R. Zeller, and P. H. Dederichs, Phys. Rev. B **52**, 11502 (1995).

[80] J. Hellsvik, D. Thonig, K. Modin, D. Iuşan, A. Bergman, O. Eriksson, L. Bergqvist, and A. Delin, Phys. Rev. B **99**, 104302 (2019).